

Barocaloric effect and materials: A review

Zi-Qi Guan(关子奇), Chang-Jiang Bao(包长江), Ji-Wei Yao(姚继伟), Nan Zhou(周楠), Yuan-Wen Feng(冯远文), Hao-Yu Wang(王皓宇), Kun Zhang(张琨), and Bing Li(李昺)

Citation: Chin. Phys. B, 2026, 35 (**7**): 070501. DOI: 10.1088/1674-1056/ae53b2
http://cpb.iphy.ac.cn; http://iopscience.iop.org/cpb

What follows is a list of articles you may be interested in

Thermodynamic and real-time dynamic properties of complex Sachdev-Ye-Kitaev model

Sizheng Cao(曹思政), Xian-Hui Ge(葛先辉), and Yi-Cheng Rui(芮易成)
Chin. Phys. B, 2026, 35 (**6**): 060512. DOI: 10.1088/1674-1056/ae48c6

Non-Hermitian many-body localization in asymmetric chains with long-range interaction

Wen Wang(王雯), Han-Ze Li(李函泽), and Jian-Xin Zhong(钟建新)
Chin. Phys. B, 2026, 35 (**6**): 060509. DOI: 10.1088/1674-1056/ae144f

Phase transition of interfacial water at low-dimensions

Wenlong Liang(梁文龙), Yujie Huang(黄雨婕), Yue Zhang(张悦), and Chunlei Wang(王春雷)
Chin. Phys. B, 2026, 35 (**2**): 020501. DOI: 10.1088/1674-1056/ae12da

Energy mechanism of the first-order superradiant phase transition in cavity-BEC system with double asymmetric pump beams

Wei Qin(覃威), Dong-Chen Zheng(郑东琛), Jia-Ying Lin(林佳颖), Yuan-Hong Chen(陈元鸿), and Renyuan Liao(廖任远)
Chin. Phys. B, 2025, 34 (**12**): 120507. DOI: 10.1088/1674-1056/addeb7

Universality of percolation at dynamic pseudocritical point

Qiyuan Shi(石骐源), Shuo Wei(魏硕), Youjin Deng(邓友金), and Ming Li(李明)
Chin. Phys. B, 2025, 34 (**4**): 040501. DOI: 10.1088/1674-1056/adaccf

---

TOPICAL REVIEW — Multiferroicity and multicaloric effects

Barocaloric effect and materials: A review

Zi-Qi Guan(关子奇)[1,2], Chang-Jiang Bao(包长江)[1], Ji-Wei Yao(姚继伟)[1], Nan Zhou(周楠)[1], Yuan-Wen Feng(冯远文)[1,2], Hao-Yu Wang(王皓宇)[1,2], Kun Zhang(张琨)[1,2], and Bing Li(李昺)[1,2,†]

[1] *Shenyang National Laboratory for Materials Science, Institute of Metal Research, Chinese Academy of Sciences, Shenyang* 110016, *China*
[2] *School of Materials Science and Engineering, University of Science and Technology of China, Shenyang* 110016, *China*

(Received 10 December 2025; revised manuscript received 6 March 2026; accepted manuscript online 18 March 2026)

As the global energy crisis and environmental issues intensify, the development of efficient and environmentally friendly novel refrigeration technology has become a significant focus in the field of scientific research and engineering. Conventional vapor compression refrigeration utilizes vapor refrigerants with high global warming potentials, which not only consume huge amounts of energy but also adversely affect the environment. In recent years, solid-state refrigeration technology has emerged as a research hotspot because of its controllable refrigerants, high energy efficiency, and environmental friendliness. Among the various refrigeration technologies that yield caloric effects through external-field-induced phase transitions, barocaloric refrigeration technology has been highly anticipated due to its low required driving pressure for refrigerant materials, large entropic change upon phase transition, and potentially high efficiency. On the other hand, many types of barocaloric materials are currently available, including intermetallic compounds, inorganic and organic materials, as well as organic–inorganic hybrid materials. Based on the barocaloric effect mechanism and the fundamental principles of various barocaloric materials, this paper summarizes the latest research in this field. It reviews the origins of the caloric effects of different types of barocaloric materials. The future development directions and application prospects of barocaloric solid-state refrigeration technology and materials are outlined.

Keywords: barocaloric effect, phase transition, entropy change, solid-state refrigeration

PACS: 05.70.Fh, 65.40.gd, 75.30.Sg, 75.85.+t

DOI: 10.1088/1674-1056/ae53b2 **CSTR:** 32038.14.CPB.ae53b2

1. Introduction

Refrigeration technology is an important part of energy consumption in modern society and is widely used in food preservation, air-conditioning systems, the medical cold chain, superconducting equipment, aerospace, and other fields.[1–3] According to statistics, the energy consumption of conventional vapor compression refrigeration technology accounts for about 20% of global electricity consumption.[3] The hydrochlorofluorocarbon (HCFC) and hydrofluorocarbon (HFC) refrigerants used in conventional vapor compression refrigeration also cause ozone layer destruction and the greenhouse effect. Furthermore, hydrofluoroolefin (HFO) refrigerants, which have a minimal environmental impact, are very expensive to produce. Therefore, the search for efficient and environmentally friendly alternative refrigeration technologies has become an urgent challenge for the global academic and industrial communities.[4–6] Solid-state caloric-effect refrigeration, as a candidate new-generation technology, realizes heat absorption and exothermic processes through reversible phase transitions of materials under the action of external fields.[7–10] Depending on the driving field, the caloric effects can be categorized into: the magnetocaloric effect (MCE),[8–10] the electrocaloric effect (ECE),[11] the elastocaloric effect (eCE),[12–16] and the barocaloric effect (BCE).[17,18] These caloric effects have been developed rapidly over the last two decades, and the adiabatic temperature change (ΔT_{ad}) of some materials has reached 10–30 K, showing performance close to that of conventional refrigeration. Among these, the hydrostatic-pressure-induced BCE (thermodynamic cycle) has gained increasing recognition as one of the most promising caloric routes in the field of practical solid-state refrigeration.[19–24]

The BCE possesses unique advantages, utilizing hydrostatic pressure — a field that can be applied uniformly, rapidly, and safely — to achieve significant reversible phase transition entropy change (ΔS_{tr}). Importantly, barocaloric materials are often associated with colossal ΔS_{tr}, originating from one or more of the following: order–disorder transitions, rotational molecular dynamics, and first-order structural transitions. This enables giant BCE to be achieved under relatively low pressures. Recent breakthroughs have demonstrated ΔS_{tr} exceeding 600 $J\cdot kg^{-1}\cdot K^{-1}$ in plastic crystals.[18] The emergence of these materials has significantly accelerated the development of barocaloric refrigeration prototypes. Despite these advantages, the practical implementation of BCE solid-state refrigeration still faces several challenges. First, many barocaloric materials exhibit a large phase transition thermal hysteresis

†Corresponding author. E-mail: bingli@imr.ac.cn

© 2026 Chinese Physical Society and IOP Publishing Ltd. All rights, including for text and data mining, AI training, and similar technologies, are reserved.

(ΔT_{hys}), which leads to energy loss and reduces the operational efficiency of cyclic refrigeration.[25–29] Second, the working temperature window of barocaloric materials is often narrow, restricting their applicability across diverse temperature conditions.[30–33] Third, the cyclic stability and fatigue resistance of barocaloric materials are currently very poor and do not meet practical application requirements.[2,17,34–37] Consequently, there has been an increasing focus on developing high-performance barocaloric materials.

Therefore, it has become an important research aim to design barocaloric materials with a low ΔT_{hys}, a long fatigue life, a large ΔS_{tr}, and a wide operating temperature range, and to develop effective strategies to improve their BCE. This includes tuning crystal chemistry, engineering molecular dynamics, coupling multicaloric effects, and optimizing pressure application mechanisms.[2,18,37] A comprehensive understanding of the structure–property relationships that govern BCE behaviors is essential for advancing solid-state refrigeration technologies toward practical, environmentally friendly, high-efficiency cooling solutions.[38–40] This review examines the physical mechanisms of barocaloric solid-state refrigeration and outlines the development of barocaloric materials.

2. Barocaloric refrigeration technology and thermodynamic cycles

2.1. Barocaloric refrigeration technology

The basis of barocaloric refrigeration technology is the use of the BCE in barocaloric materials. This effect occurs when the volume of a material changes in response to hydrostatic pressure, inducing a first-order structural phase transition and generating ΔT_{ad}. Barocaloric refrigeration technology is also one of the most promising technologies for solid-state refrigeration.[21,24,41–45] The BCE can be divided into conventional BCE and inverse BCE. The alloy NiMnIn exhibits behavior typical of the conventional BCE. When pressure is applied, driving the transformation of austenite into martensite, lattice vibration entropy (ΔS_{vib}) is negative, and magnetic entropy (ΔS_{mag}) is positive ($|\Delta S_{vib}| > |\Delta S_{mag}|$); thus, the total ΔS_{tr} is negative. Consequently, heat is released, and the temperature rises. Similarly, when pressure is removed, driving the reverse transformation of martensite to austenite, the total ΔS_{tr} is positive. Consequently, heat is absorbed, and the temperature decreases. In summary, applying pressure shifts the phase transition temperature toward a higher temperature. The $PdNMn_3$ alloy of the antiperovskite system exhibits behavior typical of the inverse BCE. Pressure drives the phase transition of the cubic phase from antiferromagnetism to ferromagnetism, accompanied by a 0.2% volume change ($\Delta V/V$). Pressure causes the phase transition temperature to shift toward a lower temperature.[27,29,46–51]

The barocaloric properties of materials are mainly characterized by the barocaloric ΔT_{ad} or entropy change (ΔS_{BCE}) induced by hydrostatic pressure, as presented in Fig. 1. Until now, it has been difficult to directly test the ΔT_{ad} values of barocaloric materials during phase transitions by applying and removing hydrostatic pressure due to the complexity of the equipment used to create the barocaloric effect and the difficulty of applying hydrostatic pressure compared to uniaxial stress. Even if the barocaloric ΔT_{ad} can be tested, the experimental values of ΔT_{ad} are far from the theoretical values. The pressure dependence of the transition temperature and entropy change can also be described by the Clausius–Clapeyron relation

$$\frac{\mathrm{d}T}{\mathrm{d}p} = \frac{\Delta V}{\Delta S}, \tag{1}$$

where ΔV and ΔS denote the discontinuous changes in volume and entropy at the phase transition, respectively.[52,53] This relation provides the appropriate thermodynamic framework for analyzing the BCE associated with first-order phase transitions. Experimentally, ΔS_{BCE} is most commonly determined using quasi-direct methods based on differential scanning calorimetry (DSC) measurements under different pressures. The corresponding ΔT_{ad} can then be estimated from the measured entropy change and heat capacity.[54–56]

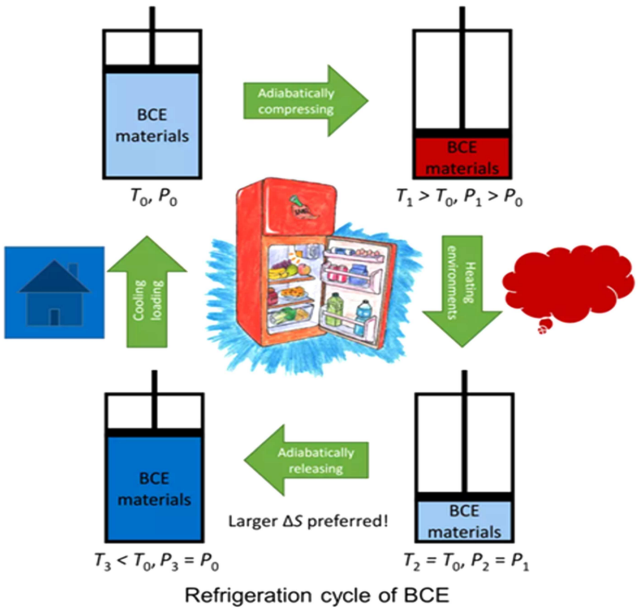


Fig. 1. Schematic diagram of the BCE.

2.2. Thermodynamic cycles

The barocaloric refrigeration system comprises a pressure cell into which the barocaloric materials are inserted, along with two heat reservoirs that must be in thermal communication with the cell to enable heat transfer. The BCE can be found in many thermodynamic cycles, such as the Carnot and Brayton cycles. The inverse Brayton cycle is the most

widely exploited configuration for caloric refrigeration applications because it requires only two field intensities and is, therefore, comparatively simple. As depicted in Fig. 2(a), within the BCE Brayton cycle, the barocaloric materials first undergo hydrostatic pressurization from p_1 to p_2, leading to a ΔT_{ad} increase in $+\Delta T_{ad,12}$. This is followed by an isobaric heat-rejection step, during which heat is transferred from the barocaloric material to the hot heat exchanger (HHEX). Subsequent isentropic depressurization from p_2 back to p_1 produces an additional ΔT_{ad} drop in $-\Delta T_{ad,34}$. Finally, the cycle closes with an isobaric heat-absorption step, in which the cooled barocaloric material absorbs heat from the cold heat exchanger (CHEX).[56,57] The BCE Brayton cycle always has a lower coefficient of performance (COP) than the Carnot cycle. Figure 2(b) shows the inverse Brayton cycle, which includes regeneration and involves the material passing through two additional steps: (2a→3) and (4a→1). This guarantees extra cooling and heating.[56]

Another widely used cycle that can easily be derived from the inverse Brayton cycle is the active barocaloric regenerative (ABR) cooling cycle, which is presented in Fig. 3. As can be seen in Fig. 3(a), the system must complete four transformations, the evolution of which is shown in Fig. 3(b). Only two levels are required for BCE to manifest (steps I and III), between which the hydrostatic pressure must change adiabatically. Steps II and IV are reserved for the passage of the heat transfer fluid (HTF) between the cold and hot heat reservoirs, which are set at temperatures T_C and T_H, respectively. Owing to the active regeneration provided by the BCE material itself, the maximum temperature span of the system can far exceed that of a Brayton cycle without regeneration, where the temperature increase is strictly limited by the intrinsic ΔT_{ad} of the barocaloric materials. Nevertheless, the hysteresis inherent in barocaloric materials compromises the adiabaticity of the process, thereby diminishing the maximum achievable ΔT_{ad}. Moreover, the ΔT_{hys} also leads to a reduction in the system's COP.[55] Therefore, enhancing the efficiency of barocaloric solid-state refrigeration technology will be a key focus of future research.

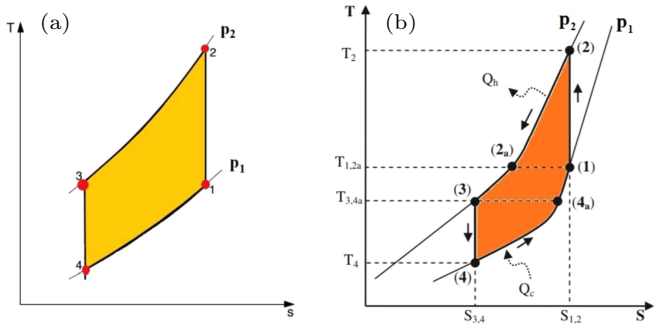


Fig. 2. (a) Inverse Brayton cycle for barocaloric cooling. (b) Inverse Brayton cycle for barocaloric cooling with regeneration.[52]

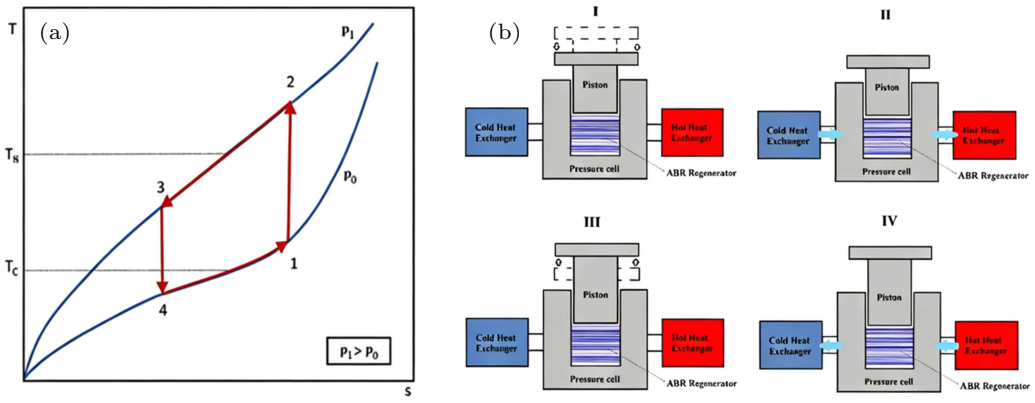


Fig. 3. The ABR cycle: (a) transformations on the temperature–entropy plane; (b) the evolution of the system.[52]

3. Classification of barocaloriceffect materials

3.1. Organic barocaloric materials

Organic compounds can be categorized into two types: chain macromolecular organics (or polymers) and small organic molecular crystals. These materials are mainly made up of elements with smaller atomic numbers, such as carbon (C), hydrogen (H), and oxygen (O). The BCE in such materials can be attributed to the transition between the ordered and disordered states of the organic chains. Recent studies have identified several key BCE compound families with unique structural features and thermal responses. These materials include plastic crystals with orientationally disordered molecules, elastomeric polymers, and macromolecular organics with solid–liquid phase transitions.[18,58–61] Among them, small-molecule plastic crystals represent one of the most thoroughly studied families. Their molecules exhibit strong pressure sensitivity due to highly disordered molecular rotations that collapse into ordered phases under compression, enabling a large BCE entropy change (ΔS_{BCE}). As shown in Fig. 4, neopentyl glycol (NPG), pentaglycerin (PG), and pentaerythritol (PE) are canonical examples; these materials show colossal entropy changes exceeding 350–700 $J \cdot kg^{-1} \cdot K^{-1}$ near RT under moderate pressure due to their highly compress-

ible, orientationally disordered high-temperature phase.[18] The barocaloric mechanism in these plastic crystals originates from the strong coupling between hydrogen bond networks and external pressure, with pressure suppressing rotational disorder and tuning intermolecular interactions, enabling large and reversible BCE.[18,62] Another significant category of organic barocaloric materials is macromolecular organics with solid–liquid phase transitions, such as n-alkanes. A slight increase in pressure of around 0.5 kbar can induce a $\Delta S_{\rm iso}$ of approximately 742 J·kg^{-1}·K^{-1}, which is comparable in magnitude to that achieved by typical vapor compression refrigeration.[63] Raman spectroscopy and theoretical calculations have revealed that twisting and random thermal movements of molecular chains are suppressed under pressure in the solid state, resulting in a large $\Delta S_{\rm iso}$. Further molecular dynamics simulations have demonstrated that n-alkane $C_{20}H_{42}$ can exhibit giant $\Delta S_{\rm iso}$ and $\Delta T_{\rm ad}$ by reducing intermolecular potential energy under compressive conditions.[64] In contrast to conventional macromolecular organic barocaloric materials, the BCE of elastomers such as natural rubber (NR) and vulcanized natural rubber (V-NR) arises from a pressure-induced entropy change rather than from a first-order phase transition. These materials exhibit BCE associated with the compression of the amorphous polymer matrix and are unrelated to crystallization and the consequent rearrangement of polymer chains. Under several hundred MPa, elastomers can yield a $\Delta S_{\rm iso}$ of about 50–200 J·kg^{-1}·K^{-1} and a $\Delta T_{\rm ad}$ of 10–30 K.[62–67]

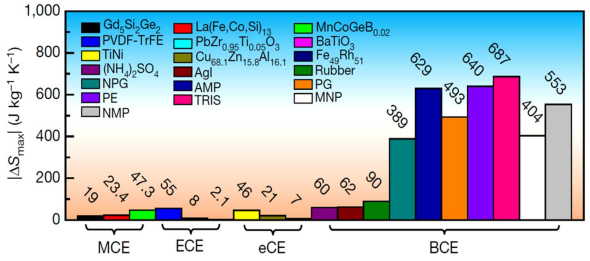


Fig. 4. Entropy changes of plastic crystal materials and typical refrigeration materials.[18]

These organic systems share several key advantages: (i) extremely high entropy changes due to large latent heat and molecular disorder; (ii) broad chemical tunability through molecular design, chain length modification, or hydrogen bond engineering; (iii) mechanical flexibility and low density; (iv) absence of critical raw metals or inorganic species, making them environmentally friendly. However, they also face significant challenges, including large $\Delta T_{\rm hys}$ in many plastic crystals, low thermal conductivity that limits heat exchange rates, mechanical fatigue in polymer-based systems, and issues of leakage and volume change for organic solid–liquid phase transition compounds.

3.2. Organic–inorganic hybrid barocaloric materials

Organic–inorganic hybrid materials are single-phase, solid-state compounds that incorporate both inorganic and organic groups within the same crystal structure. The variation in degrees of freedom within these materials is the primary source of the BCE. These degrees of freedom can be categorized as follows: rotational, translational, orientational, and conformational. According to their coordination dimensionality, hybrid materials can be classified as three-dimensional (3D), two-dimensional (2D), one-dimensional (1D), or zero-dimensional (0D), as displayed in Fig. 5.[68–70]

Organic–inorganic hybrid perovskite materials demonstrate a remarkable BCE, primarily due to pressure-induced structural phase transitions. Exceptionally high-pressure sensitivity has been observed in 3D hybrid materials such as [TPrA][Mn(dca)$_3$], where a phase transition occurs at a pressure (dT/dP) of 23.1 K·kbar^{-1}. Notably, the pressure required to drive these transitions is extremely low. Applying minimal hydrostatic pressure of just 70 bar induces a significant $\Delta S_{\rm iso}$ of 37 J·kg^{-1}·K^{-1}. This effect is primarily due to the order–disorder transition of organic cations and their off-center displacement.[71] In contrast, 2D hybrid materials exhibit a substantially larger BCE. For example, $(DA)_2MnCl_4$ and $(C_{10}H_{21}NH_3)_2MnCl_4$ achieve a reversible, colossal $\Delta S_{\rm iso}$ of around 250 J·kg^{-1}·K^{-1} at an operating pressure below 1 kbar, which far exceeds that of their 3D counterparts.[70,72] These 2D hybrid materials offer several advantages, including high pressure sensitivity ($dT/dP \approx 28$ K·kbar^{-1}) and minimal $\Delta T_{\rm hys}$. The large entropy change is due to the significant transformation of organic chains from an ordered, rigid state to a disorganized, flexible state during the phase transition, coupled with the reorientation of alkylammonium cations within the metal-halide frameworks. One-dimensional hybrid materials typically consist of isolated columns or chains of inorganic metal cations that are interconnected by organic (and sometimes inorganic) ligands. These chains are linked via weak bonds and can accommodate other organic or inorganic species within their structure.[73] Their general formula is $M(L)(L)\cdot xH_2O$, where M is a transition metal cation, and L is a different organic ligand. Examples of such compounds include [Cu(hyetrz)$_3$]·3H$_2$O. Hybrid materials that do not exhibit strong chemical interactions between their organic and inorganic components are referred to as 0D or ionic/molecular hybrids. These materials interact only through weak hydrogen bonding, van der Waals forces, π–π interactions, or other electrostatic interactions.[74] Alkylammonium tetrahalometallate salts belong to this category. For example, the compound $[(CH_3)_3S][FeCl_4]$ undergoes a phase transition at 326 K, displaying relatively low $\Delta T_{\rm hys}$ (approximately 4.0 K) and a significant entropy change (approximately 140 J·kg^{-1}·K^{-1}).[75]

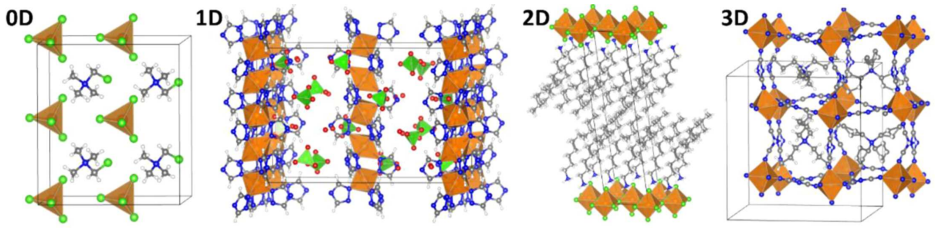


Fig. 5. Organic–inorganic hybrid materials with different coordination dimensionalities.[52]

Organic–inorganic barocaloric materials offer several advantages, including high structural and chemical stability, large volume changes upon phase transitions, and correspondingly significant BCEs. Their mature synthesis routes enable the preparation of large, high-quality samples suitable for device-level development. However, these materials also exhibit notable limitations. Their rigid lattices and low compressibility typically require high external pressures to drive phase transitions, and many organic-inorganic hybrid materials exhibit large phase transition $\Delta T_{\rm hys}$, which reduces reversibility and overall cycle efficiency. In addition, the use of scarce or heavy elements in some systems raises costs and environmental concerns.

3.3. Intermetallic compounds as barocaloric materials

Intermetallic compounds consist primarily of metals, occasionally containing nonmetallic elements. These compounds primarily exhibit metallic bonding; examples include MnNiGe, MnCoGe, Ni–Mn–X (X = Ga, Sn, Sb, In, Ti), Mn_3NiN, and Mn_3GaN.[25,28,62,76–80] Some of these compounds exhibit the conventional BCE, while others exhibit the inverse BCE. These compounds exhibit strong coupling during phase transitions due to their ferromagnetic order, ferroelastic order, lattice structure, and volume changes. This provides a rich basis for tunable physical properties in the field of solid-state refrigeration. In addition, these compounds, which exhibit both ferromagnetic and ferroelastic order, can undergo multi-field-modulated phase transitions and demonstrate multicaloric effects.[2,20,78] Figure 6 presents the results of Wei *et al.*[80] that the $Ni_{35.5}Co_{14.5}Mn_{35}Ti_{15}$ alloy can achieve a larger $\Delta S_{\rm BCE}$ by the simultaneous action of dual fields, hydrostatic field and magnetic field. The reversible $\Delta S_{\rm BCE}$ of the alloy increased from 8.5 J·kg^{-1}·K^{-1} under a single stress field to 22.8 J·kg^{-1}·K^{-1} under a 3 T magnetic field and 1 kbar pressure. When simultaneously driven by double fields, the reversible refrigeration working temperature range of the alloy is also nearly doubled. This suggests that barocaloric materials with multiferroic properties can be driven by multiple fields to modulate the phase transition, thereby improving the BCE and the operating temperature range of the material. Similar phenomena have been observed in $MM'X$ and M_3XA alloys.[27–29,62,65]

Although the phase transitions of intermetallic barocaloric compounds can be modulated by a double field, the phase transition entropy change of such materials is usually small and much lower than that of the plastic crystal barocaloric materials that have emerged in recent years.[2,3,18]

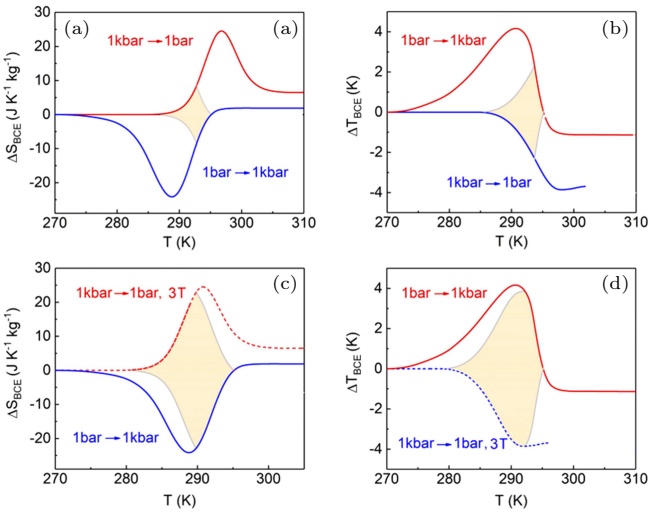


Fig. 6. Reversible entropy and adiabatic temperature changes of $Ni_{35.5}Co_{14.5}Mn_{35}Ti_{15}$ alloy under single and multiple fields.[80]

3.4. Spin crossover barocaloric materials

Early investigations of the caloric properties of spin crossover (SCO) transitions were carried out in the absence of applied pressure, primarily through heat capacity measurements under ambient conditions. In 1974, Sorai provided the first heat capacity characterization of abrupt SCO transitions in the compounds $[Fe(phen)_2(NCS)_2]$ and $[Fe(phen)_2(NCSe)_2]$. They found latent heats corresponding to entropy changes of approximately 50 J·K^{-1}·mol^{-1}.[81] Importantly, only a small fraction of this entropy change ($\sim$ 13 J·K^{-1}·mol^{-1}) could be attributed to the magnetic contribution, indicating that lattice, vibrational, and configurational degrees of freedom dominate the thermodynamics of the transition. Similar conclusions were reached in later heat capacity studies by Kaji of $[Fe(2\text{-pic})_3]Cl_2$·EtOH, a system exhibiting an apparent two-step SCO transition.[82] When the normal density of SCO complexes is confirmed, these unoptimized entropy changes correspond to values on the order of 100 J·kg^{-1}·K^{-1} or 0.2 J·K^{-1}·cm^3, which would be described as large caloric effects if they could be released by an applied stimulus, such as pressure. The pressure-induced generic SCO transition of SCO materials is illustrated in Fig. 7. The low-spin (LS) state

of an SCO compound typically has a lower volume than the high-spin (HS) state. In such cases, the effect of hydrostatic pressure is to stabilize the LS state.

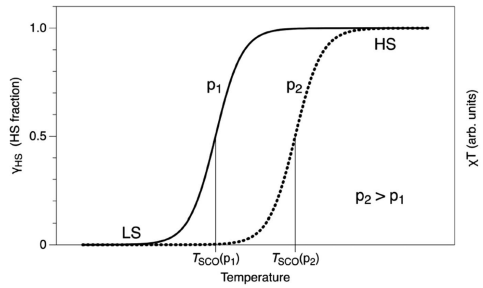


Fig. 7. Schematic of the typical LS state-stabilizing effect of hydrostatic pressure on an SCO compound.[52]

The pressure required to induce phase transitions in these materials is generally low. High-pressure calorimetry of the SCO compound $Fe[HB(tz)_3]_2$ reveals detectable entropy changes at pressures as low as 1 MPa.[53] A ΔS_{iso} of 99 $J{\cdot}kg^{-1}{\cdot}K^{-1}$ and a ΔT_{ad} of 2 K are achieved under a hydrostatic pressure of 15 MPa. Similarly, the molecular crystal $[FeL_2][BF_4]_2$ exhibits a ΔT_{ad} of 3 K under a pressure of 30 MPa, which is associated with a first-order transition between the LS and HS states.[83] For $[Fe(hyptrz)_3]A_2{\cdot}H_2O$, applying a pressure of approximately 9 MPa produces a ΔS_{iso} of about 56 $J{\cdot}kg^{-1}{\cdot}K^{-1}$.[84] The large $\Delta V/V$ during the spin-state transition leads to a large lattice entropy contribution, reflecting strong coupling between lattice and electronic states in $Fe^{2+}N_6$. Consequently, a giant BCE can be observed. From a broader perspective, SCO materials offer several advantages as barocaloric materials, including large ΔS_{iso}, high dT/dP, and chemical tunability of transition temperatures. However, they also present notable challenges, such as thermal hysteresis, mechanical fragility, and limited thermal conductivity.

3.5. Ionic compounds as barocaloric materials

Ionic compounds consist of cations (cationic groups) and anions (anionic groups), and their phase transitions typically include ionic-order transitions as well as ferroelectric or ferromagnetic transitions. In particular, the presence of negative thermal expansion associated with ferromagnetic or ferroelectric phase transitions can give rise to a BCE. This behavior has been observed in several ionic compounds, including NiS, $BaTiO_3$, KPF_6, and $(NH_4)_2SO_4$.[62,79,80,85] The primary advantages of ionic compounds are their abundant constituent elements, widespread availability, and low cost. In addition, these materials offer high structural design flexibility, enabling phase transition temperatures and ΔT_{hys} to be adjusted through ion exchange or doping. Significant BCEs can typically be achieved at relatively low pressures (tens to hundreds of MPa). Most ionic compounds are nontoxic and highly stable, making them ideal for large-scale manufacturing.[62,80]

Recent studies have also demonstrated that certain ionic compounds, such as KPF_6, possess high-pressure phases across a broad temperature range, as illustrated in Fig. 8. This enables these materials to exhibit a BCE from room temperature down to cryogenic temperatures of 4 K. This discovery also marks the first finding of a solid-state refrigeration material effective at all temperatures.[19] However, these materials also face certain challenges, including a large phase transition ΔT_{hys}, limited cyclic stability, and relatively low thermal conductivity. These factors somewhat constrain their efficiency in high-frequency refrigeration cycles. Nevertheless, ionic compounds are considered important candidate material systems for solid-state pressure-driven refrigeration technology due to their large enthalpy change and structural tunability.[62–64,85]

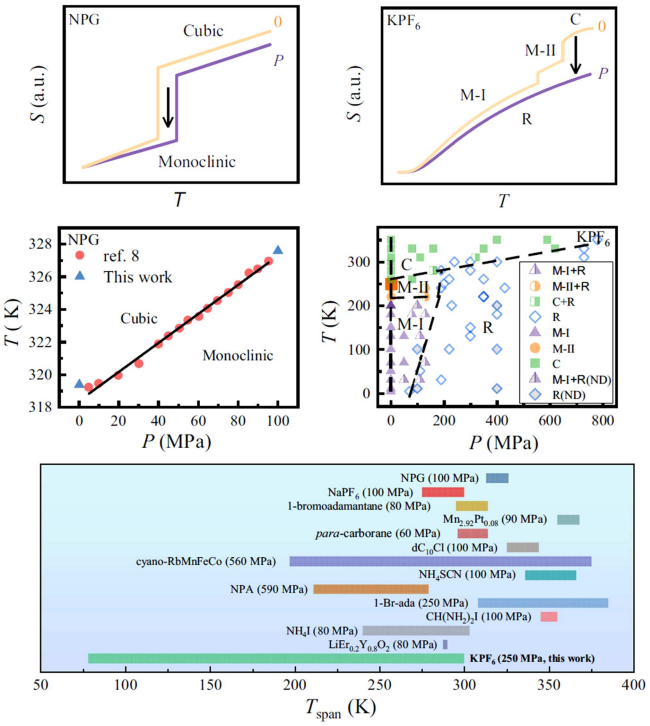


Fig. 8. Schematic entropy–temperature curves (a) and high-pressure phase diagrams (b) for NPG. Entropy–temperature curves (c) and high-pressure phase diagrams (d) for KPF_6. (e) Comparison between the operating temperature ranges of regular BCE materials with that of KPF_6.[19]

Ionic compounds, similarly to intermetallic compounds, exhibit both ferroelectric and ferroelastic order during phase transitions and can also be used to modulate caloric effects through electric- and stress-field-driven phase transitions. Although a dual field can modulate the phase transitions of intermetallic and ionic compounds, the phase transition entropy change of such materials is usually small and is much lower than that of the plastic crystal barocaloric materials that have emerged in recent years.[2,3,18] In addition, intermetallic compounds usually have a larger driving field for the phase transition, and their dT/dP sensitivity is much lower than that of organic or inorganic barocaloric materials. Table 1 lists

the BCE parameters of different barocaloric materials to compare their performance more directly. In general, intermetallic compounds have high thermal conductivity, but the application of these materials is hindered by high driving pressures and low BCE. In contrast, organic and hybrid barocaloric materials operate at low pressures and have excellent reversibility and flexibility, although their heat transfer capability is lower. Future developments will focus on combining the advantages of these materials through composite architectures, microstructural design, and multifield coupling strategies, with the aim of achieving high-performance, durable, and eco-friendly solid-state refrigeration.

Table 1. Performance parameters of typical barocaloric materials. Here, (p), (ΔS_{rve}), and (RC) are the maximum applied pressure, reversible ΔS_{BCE}, and refrigeration capacity of the listed materials, respectively.

Material	ΔT_{ad} (K)	ΔS_{rve} ($\mathrm{J\cdot kg^{-1}\cdot K^{-1}}$)	RC ($\mathrm{J\cdot kg^{-1}}$)	ΔT_{hys} (K)	P (MPa)	ΔS_{BCE} ($\mathrm{J\cdot kg^{-1}\cdot K^{-1}}$)	$\mathrm{d}T/\mathrm{d}P$ ($\mathrm{K\cdot MPa^{-1}}$)	Thermal conductivity ($\mathrm{W\cdot m^{-1}\cdot K^{-1}}$)	Ref.
NPG	30	–	24138	24	91	389	0.13	0.37	[18,85]
PG	10	490	4948	11	240	490	0.09	0.36	[86,87]
AMP	16	–	10596	55	200	690	0.08	–	[86,88]
$C_{10}H_{15}Br$	10.4	20	–	9	60	88.3	0.25	0.684	[87]
$C_{10}H_{15}Cl$	–	208	14542	8.4	240	208	0.27	–	[90]
$(C_{10}H_{21}NH_3)_2MnCl_4$	12	250	8373	8.2	250	250	0.25	0.3	[62]
[TPrA][Mn(dca)$_3$]	4.1	30.5	479	2.8	7	30.5	0.19	0.25	[71]
$[FeL_2][BF_4]_2$	4.5	–	–	4	430	76	0.152	1.4	[83]
$Ni_{35.5}Co_{14.5}Mn_{35}Ti_{15}$	4.2	22.8	–	6	100	24.2	0.058	–	[80]
$Gd_5Si_2Ge_2$	1.3	–	149	5	300	6.2	0.035	5.64	[86,89]
$Ni_{49.26}Mn_{36.08}In_{14.66}$	4.5	10	104	4.4	300	24.4	0.018	–	[38]
$LaFe_{11.33}Co_{0.47}Si_{1.2}$	2.2	–	183	–	$\sim$240	8.7	–	6–7	[24]
(MnNiGe)(FeCoGe)	5.2	19.3	255	6.4	100	32.8	0.069	–	[29]
NH_4SCN	26	70	3755	28	100	128.7	0.258	–	[2]
$BaTiO_3$	3	–	15.5	4	390	1.47	0.056	0.8	[91]
AgI	18	60	1085	25	$\sim$420	60	0.135	0.2	[92]
NH_4I	–	71	3046	26.1	80	71	0.79	–	[93]

4. Outlook

In summary, the BCE represents a promising pathway toward next-generation solid-state refrigeration, offering environmentally friendly alternatives to conventional vapor-compression systems. However, challenges such as large ΔT_{hys}, limited reversibility, and high driving fields still hinder the practical applications of barocaloric materials. Future research should focus on developing barocaloric materials that exhibit strong and reversible thermal responses with high thermal conductivity, low driving fields, and enhanced cyclic stability. The simultaneous application of multiple external fields (magnetic, electric, and mechanical) has demonstrated clear advantages over single-field operation. Multifield coupling can reduce phase transition barriers, suppress ΔT_{hys}, and enhance both ΔT_{ad} and ΔS_{iso}. This synergy enables tunable control of caloric effects and facilitates continuous, wide-temperature cooling.

At present, it is difficult for existing different types of barocaloric materials to achieve a comprehensive trade-off in barocaloric performance, as they are unable to deliver outstanding performance across all key BCE parameters simultaneously. Therefore, in the future, we should consider preparing composite barocaloric materials with excellent overall properties and more efficient pressure-based solid-state refrigeration systems. The combination of synergistic field coupling and intelligent materials design offers a viable route to high-performance and carbon-free barocaloric solid-state refrigeration.

Acknowledgements

This work is financially supported by the National Natural Science Foundation of China (Grant Nos. 52425107, 52401253, and 52571021), the Key Research Program of Frontier Sciences of the Chinese Academy of Sciences (Grant No. ZDBS-LYJSC002), the Innovation Fund of the Institute of Metal Research, Chinese Academy of Sciences (Grant No. 2024-PY05), the Natural Science Foundation of Liaoning Province (Grant No. 2024-BSBA-41), and the Postdoctoral Fellowship Program of the China Postdoctoral Science Foundation (Grant No. GZC20232741).

References

[1] Ding Y L, Briggs C, Okazaka T, Thess A and Wang R Z 2021 *Climate change: Science and solutions Briefing* **3** 1
[2] Zhang Z, Li K, Lin S C, Song R Q, Yu D H, Wang Y D, Wang J F, Kawaguchi S, Zhang Z, Yu C Y, Li X D, Chen J, He L H, Mole R, Yuan B, Ren Q Y, Qian K, Cai Z L, Yu J G, Wang M C, Zhao C Y, Tong X, Zhang Z D and Li B 2023 *Sci. Adv.* **9** eadd0374
[3] Zhang K, Song R Q, Qi J, Zhang Z, Yu C Y, Li K, Zhang Z D and Li B 2022 *Adv. Funct. Mater.* **32** 2112622
[4] McLinden M O, Brown J S, Brignoli R, Kazakov A F and Domanski P A 2017 *Nat. Commun.* **8** 14476
[5] European Commission 2015 *Molenbroek, Savings and Benefits of Global Regulations for Energy Efficient Products* (Final Report)
[6] Sooben D, Purohit N, Mohee R, Meunier F and Dasgupta M S 2019 *Int. J. Refrig.* **103** 264

[7] Xu X, Xie W F, Li F B, Niu C, Li M and Wang H 2024 *Phys. Rev. Appl.* **22** 014036
[8] Niu C, Li F B, Xu X, Xie W F, Zhai G W, Li M and Wang H 2024 *Appl. Phys. Lett.* **124** 103905
[9] Tegus O, Brück E, Buschow K H J and de Boer F R 2002 *Nature* **415** 150
[10] Li Z B, Jiang Y W, Li Z Z, Sanchez Valdes C F, Sanchez Llamazares J L, Yang B, Zhang Y D, Esling C, Zhao X and Zuo L 2018 *IUCrJ* **5** 54
[11] Mischenko A S, Zhang Q, Scott J F, Whatmore R W and Mathur N D 2006 *Science* **311** 1270
[12] Bonnot E, Romero R, Mañosa L, Vives E and Planes A 2008 *Phys. Rev. Lett.* **100** 125901
[13] Cui J, Wu Y M, Muehlbauer J, Hwang Y, Radermacher R, Fackler S, Wuttig M and Takeuchi I 2012 *Appl. Phys. Lett.* **101** 073904
[14] Tušek J, Engelbrecht K, Millán-Solsona R, Mañosa L, Vives E, Mikkelsen L P and Pryds N 2015 *Adv. Energy Mater.* **5** 1500361
[15] Cong D Y, Xiong W X, Planes A, Ren Y, Mañosa L, Cao P Y, Nie Z H, Sun X M, Yang Z, Hong X F and Wang Y D 2019 *Phys. Rev. Lett.* **122** 255703
[16] Liu C, Li D, Li Z B, Yang B, Yan H L, Li J R, Li Z, Zhao X and Zuo L 2021 *Appl. Phys. Lett.* **118** 103904
[17] Qian K, Lin S C, Zhang Z, Li B, Peng Y C, Li Y J and Zhao C Y 2024 *Cell Rep. Phys. Sci.* **5** 101981
[18] Li B, Kawakita Y, Ohira-Kawamura S, Sugahara T, Wang H, Wang J F, Chen Y N, Kawaguchi S, Kawaguchi S, Ohara K, Li K, Yu D H, Mole R, Hattori T, Kikuchi T, Yano S, Zhang Z, Zhang Z, Ren W J, Lin S C, Sakata O, Nakajima K and Zhang Z D 2019 *Nature* **567** 506
[19] Zhao X T, Zhang Z, Hattori T, Wang J T, Li L L, Jia Y T, Li W W, Xue J N, Fan X Y, Song R Q, Zhu J L, Liu P T, Chen X Q, Zhang Z D and Li B 2025 *Nat. Commun.* **16** 7713
[20] Mañosa L, Jarque-Farnos S, Vives E and Planes A 2013 *Appl. Phys. Lett.* **103** 211904
[21] Seo J, McGillicuddy R D, Slavney A H, Zhang S, Ukani R, Yakovenko A A, Zheng S L, Mason J A 2022 *Nat. Commun.* **13** 2536
[22] Gao Y H, Wang D H, Hu F X, Huang Q Z, Song Y T, Yuan S K, Yuan Z Y, Wang B J, Yu Z B, Zhou H B, Kan Y, Lin Y, Wang J, Li Y L, Liu Y, Chen Y Z, Sun J R, Zhao T Y and Shen B G 2024 *Nat. Commun.* **15** 1838
[23] Song R Q, Zhang Z D and Li B 2022 *J. Refrig.* **43** 35
[24] Mañosa L, Gonzalez-Alonso D, Planes A, Barrio M, Tamarit J L, Titov I S, Acet M, Bhattacharyya A and Majumdar S 2011 *Nat. Commun.* **2** 595
[25] Kuang Y F, Tao K, Yang B, Tong P, Zhang Y, Sun Z G, Zhang K W, Wang D H, Hu J F and Zuo L 2024 *Int. J. Min. Met. Mater.* **31** 2528
[26] Neaton J B, Ederer C, Waghmare U V, Spaldin N A and Rabe K M 2005 *Phys. Rev. B* **71** 014113
[27] Kuang Y F, Hao X W, Zhang Z, Yang B, Li B, Li Z B, Yan H L, Zhang Y D, Esling, C, Zhao X and Zuo L 2022 *J. Magn. Magn. Mater.* **543** 168639
[28] Qiao K, Hu F X, Liu Y, Li J, Kuang H, Zhang H R, LiangW H, Wang J, Sun J R and Shen B G 2019 *Nano Energy* **59** 285
[29] Kuang Y F, Qi J, Xu H J, Yang B, Li Z B, Yan H L, Zhang Y D, Esling, C, Zhao X and Zuo L 2021 *Scripta Mater.* **200** 113908
[30] Gschneidner K A Jr, Pecharsky V K and Tsokol A O 2005 *Rep. Prog. Phys.* **68** 1479
[31] Shen B G, Sun J R, Hu F X, Zhang H W and Cheng Z H 2009 *Adv. Mater.* **21** 4545
[32] Wang Y X, Gong W, Su Y H and Li B 2024 *Acta Metall. Sin.* **60** 1001
[33] Moya X, Kar-Narayan S and Mathur N D 2014 *Nat. Mater.* **13** 439
[34] Liu J, Gong Y, You Y, You X, Huang B, Miao X, Xu G, Xu F and Bruck E 2019 *Acta Mater.* **174** 450
[35] Scheibel F, Gottschall T, Taubel A, Fries M, Skokov K P, Terwey A, Keune W, Ollefs K, Wende H, Farle M, Acet M, Gutfleisch O and Gruner M E 2018 *Ener. Technol.* **6** 1397
[36] Gràcia-Condal A, Gottschall T, Pfeuffer L, Gutfleisch O, Planes A and Mañosa L 2020 *Appl. Phys. Rev.* **7** 041406
[37] Hou H L, Qian S X and Takeuchi I 2022 *Nat. Rev. Mater.* **7** 633
[38] Mañosa L, *et al.* 2010 *Nat. Mater.* **9** 478
[39] Vopson M M 2012 *Solid State Commun.* **152** 2067
[40] Mañosa L, Planes A and Acet M 2013 *J. Mater. Chem. A* **1** 4925
[41] Li B and Zhang Z D 2021 *Sci. Sin. Phys. Mech. As.* **51** 067505
[42] Pecharsky V K and Gschneidner K A 1997 *Phys. Rev. Lett.* **78** 4494
[43] Bruck E 2005 *J. Phys. D: Appl. Phys.* **38** R381
[44] Nehan P Z Z, Vitayaya O, Munazat D R, Manawan M T E, Darminto D and Kurniawan B 2024 *Phys. Chem. Chem. Phys.* **26** 14476
[45] Qian S X, Catalini D, Muehlbauer J, Liu B Y, Mevada H, Hou H L, Hwang Y, Radermacher R and Takeuchi I 2023 *Science* **380** 722
[46] Huang X M, Wang L D, Liu H X, Yan H L, Jia N, Yang B, Li Z B, Zhang Y D, Esling C, Zhao X and Zuo L 2019 *Intermetallics* **113** 106579
[47] Liu C, Li Z, Wang H, Wang Y, Yang B, Yan H, Cong D, Zhao X and Zuo L 2022 *ACS Appl. Energy Mater.* **5** 12953
[48] Tušek J, Engelbrecht K, Mikkelsen L P and Pryds N 2015 *J. Appl. Phys.* **117** 124901
[49] Huang X M, Zhao Y, Yan H L, Jia N, Yang B, Li Z, Zhang Y, Esling C, Zhao X, Ren Q, Tong X and Zuo L 2023 *Scr. Mater.* **234** 115544
[50] Dang P, Ye F, Zhou Y, Ding L, Pang J, Zhang L, Ding X, Sun J, Dai S, Lookman T and Xue D 2022 *Acta Mater.* **229** 117802
[51] Kim Y H, Jo M G, Park J W, Park H K and Han H N 2018 *Scr. Mater.* **144** 48
[52] Lloveras P 2023 *Barocaloric Effects in the Solid State: Materials and Methods* (Bristol: IOP Publishing)
[53] Seo J, Braun J D, Dev V M and Mason J A 2022 *J. Am. Chem. Soc.* **144** 6493
[54] Rožič B and Kutnjak Z 2009 *Proceedings of the 2009 SEM Annual Conference & Exposition on Experimental & Applied Mechanics*, Albuquerque, New Mexico, USA
[55] Aprea C, Greco A, Maiorino A and Masselli C 2020 *Energy* **190** 116404
[56] Aprea C, Greco A, Maiorino A and Masselli C 2018 *Therm. Sci. Eng. Progr.* **6** 370
[57] Greco A, Aprea C, Maiorino A and Masselli C 2019 *Int. J. Refrig.* **106** 66
[58] Bom N M, Imamura W, Usuda E O, Paixao L S and Carvalho A M G 2018 *Acs. Macro. Lett.* **7** 31
[59] Franco V, Blázquez J S, Ipus J J, Law J Y, Moreno-Ramírez L M and Conde A 2018 *Prog. Mater. Sci.* **93** 112
[60] Cheng P T, Chen Z H, Zhang C L, Zhang Z M, Li B and Wang D H 2025 *Chin. Phys. B* **34** 036801
[61] Neese B, Chu B, Lu S G, Wang Y, Furman E and Zhang Q M 2008 *Science* **321** 821
[62] Sun Y, An S H, Gao Y H, Yu Z B, Yuan X L, Ma Z J, Shi K W, Hu F X and Wang C 2025 *J. Mater. Chem. A* **13** 6152
[63] Lin J, Tong P, Zhang K, Tao K, Lu W, Wang X, Zhang X, Song W and Sun Y 2022 *Nat. Commun.* **13** 1
[64] Miliante C M, Christmann A M, Soares R P, Bocca J R, Alves C S, Carvalho A M G and Muniz A R 2022 *J. Mater. Chem. A* **10** 8344
[65] Tao K, Song W, Lin J, Zhang X, Tong P, Zhang Z, Qi J, Li B, Ling L, Ma L and Sun Y 2021 *Scr. Mater.* **203** 114049
[66] Miliante C M, Christmann A M, Usuda E O, Imamura W, Paixao L S, Carvalho A M G and Muniz A R 2020 *Macromolecules* **53** 2606
[67] Carvalho A M G, Imamura W, Usuda E O and Bom N M 2018 *Eur. Polym. J.* **99** 212
[68] Rao C N R, Cheetham A K and Thirumurugan A 2008 *Matter* **20** 083202
[69] García-Ben J, McHugh L N, Bennett T D and Bermúdez-García J M 2022 *Chem. Rev.* **455** 214337
[70] Lloveras P 2023 *Barocaloric Effects in the Solid State Materials and methods.* **6** 1 (IOP Publishing)
[71] Salgado-Beceiro J, Nonato A, Silva R X, García-Fernández A, Sánchez-Andújar M, Castro-Garcia S, Stern-Taulats E, Señarís-Rodríguez M A, Moya X and Bermúdez-García J M 2020 *Mater. Adv* **1** 3167
[72] Yaghi O M, Li G and Li H 1995 *Nature* **378** 703
[73] Garcia Y, Van Koningsbruggen P J, Bravic G, Guionneau P, Chasseau D, Cascarano G L, Moscovici J, Lambert K, Michalowicz A and Kahn O 1997 *Inorg. Chem.* **36** 6357
[74] Chen X G, Zhang Y Z, Sun D S, Gao J X, Hua X N and Liao W Q 2019 *Dalt. Trans.* **48** 11292
[75] Salgado-Beceiro J, Bermúdez-García J M, Llamas-Saiz A L, Castro-García S, Señarís-Rodríguez M A, Rivadulla F and Sánchez-Andújar M 2020 *J. Mater. Chem. C* **8** 13686
[76] Aznar A, Gracia-Conda A, Planes A, Lloveras P, Barrio M, Tamarit J L, Xiong W, Cong D, Popescu C and Manosa L 2019 *Phys. Rev. Mater.* **3** 044406

[77] Aznar A, Lloveras P, Kim J Y, Stern-Taulats E, Barrio M, Lluis Tamarit J, Sanchez-Valdes C F, Sanchez Llamazares J L, Mathur N D and Moya X 2019 *Adv. Mater.* **31** 1903577
[78] Matsunami D, Fujita A, Takenaka K and Kano M 2015 *Nat. Mater.* **14** 73
[79] Boldrin D, Mendive-Tapia E, Zemen J, Staunton J B, Hansen T, Aznar A, Tamarit J L, Barrio M, Lloveras P, Kim J, Moya X and Cohen L F 2018 *Phys. Rev. X* **8** 041035
[80] Wei Z, Shen Y, Zhang Z, Guo J, Li B, Liu E, Zhang Z and Liu J 2020 *APL Mater.* **8** 051101
[81] Sorai M and Seki S 1974 *J. Phys. Chem. Solids* **35** 555
[82] Kaji K and Sorai M 1985 *Thermochim. Acta* **88** 185
[83] Vallone S P, Tantillo A N, dos Santos A M, Molaison J J, Kulmaczewski R, Chapoy A, Ahmadi P, Halcrow M A and Sandeman K G 2019 *Adv. Mater.* **31** 1807334
[84] von Ranke P J, Alho B P, Ribas R M, Nobrega E P, Caldas A, de Sousa V S R, Colaco M V, Marques L F, Rocco D L and Ribeiro P O 2018 *Phys. Rev. B* **98** 224408
[85] Lloveras P, Aznar A, Barrio M, Negrier P, Popescu C, Planes A, Manosa L, Stern-Taulats E, Avramenko A, Mathur N D, Moya X and Tamarit J L 2019 *Nat. Commun.* **10** 1803
[86] Aznar A, Lloveras P, Barrio M, Negrier P, Planes A, Manosa L, Mathur N D, Moya X and Tamarit J L 2020 *J. Mater. Chem. A* **8** 639
[87] Bao C J, Guan Z Q, Li Z, Wang H, Feng Y, Guo Q, Zhang K, Wang Y, Zuo L, Li B 2025 *J. Mater. Sci. Technol.* **218** 88
[88] Chandra D, Ding W, Lynch R A, Tomilinson J J 1991 *J. Less Common Metals.* **168** 159
[89] Yuce S, Barrio M, Emre B, Stern-Taulats E, Planes A, Tamarit J L, Mudryk Y, Gschneidner K A, Jr. Pecharsky V K and Manosa L 2012 *Appl. Phys. Lett.* **101** 071906
[90] Aznar A, Negrier P, Planes A, Manosa L, Stern-Taulats E, Moya X, Barrio M, Tamarit J L and Lloveras P 2021 *Appl. Mater. Today* **23** 101023
[91] Stern-Taulats E, Lloveras P, Barrio M, Defay E, Egilmez M, Planes A, Tamarit J L, Mañosa L, Mathur N D and Moya X 2016 *APL Mater.* **4** 091102
[92] Aznar A, Lloveras P, Romanini M, Barrio M, Tamarit J L, Cazorla C, Errandonea D, Mathur N D, Planes A, Moya X and Mañosa L 2017 *Nat. Commun.* **8** 1851
[93] Ren Q Y, Qi J, Yu D H, Zhang Z, Song R Q, Song W L, Yuan B, Wang T H, Ren W J, Zhang Z D, Tong X and Li B 2022 *Nat. Commun.* **13** 2293